

Invited Paper

Surface and Interface Analysis using High Energy Electron Spectroscopy

László Kövér

Institute of Nuclear Research of the Hungarian Academy of Sciences (MTA ATOMKI)

18/c Bem tér, H-4026 Debrecen, Hungary

*(*lkover@atomki.hu)*

(Received: November 26, 2007; Accepted: December 19, 2007)

High resolution spectroscopy of high (2-15 keV) energy electrons induced by photon or electron beams from solids has shown a fast progress recently, concerning both experiment and theory. High energy resolution spectroscopy of electrons backscattered from solids provides an effective tool for deriving important physical parameters characterizing the electron transport processes. The energy dependence of these parameters is shown. Central problems of quantitative surface/interface analytical applications of hard X-ray induced electron spectroscopy, including non-dipole effects in photoionization, separability and intensity ratios of contributions due to various processes attributable to atomic excitations accompanying photoionization, excitations occurring during electron transport and escape of electrons from surface layers or caused by the appearance of the core hole(s), are discussed. Examples are shown from our recent results connected with the quantitative analysis of hard X-ray excited photoelectron spectra and resonant and non-resonant Auger electron spectra emitted from 3d transition metals and semiconductors.

1. Introduction

For revealing properties of bulk and interface structures, Hard X-ray PhotoElectron Spectroscopy (HAXPES) is expected to be used increasingly in the near future, due to the decreased surface- and increased bulk sensitivity. The extended information depth makes accessible deeply buried interfaces and their electronic structures and new possibilities open for nondestructive concentration depth profiling in a broad depth range. Highly intense photon beams of third or fourth generation synchrotron beams can compensate for the low photoionization cross sections. In addition, using grazing incidence photons, HAXPES can provide extreme surface sensitivity. However, to obtain accurate information on electronic structure and quantitative analytical applications, a deeper knowledge on hard X-rays induced ionization and excitation processes as well as on transport of energetic electrons in solids is needed.

2. Information on parameters of electron transport in solids – from high energy resolution spectra of back-scattered electrons

There are different types of excitations accompanying photoionization in solids, causing an energy loss of the signal electron: upon creation of the core hole, electrons can be excited from occupied to unoccupied states (shake up/off) and collective (plasmon) excitations can also take place. These excitations are called intrinsic excitations. During electron transport within the solid, extrinsic excitations can occur in the bulk or at surface/interface crossings, e.g. bulk or surface plasmon creation. Multiple excitations are probable and interferences can appear between surface and bulk, as well as between extrinsic and intrinsic excitations. Electron transport in solids can be characterized by physical parameters and distributions useful for simulation or interpretation of experimental electron spectra. Some important physical quantities used in describing electron transport in solids are: IMFP (inelastic mean free path), the mean free path of electrons for inelastic scattering, SEP (surface excitation parameter), the average number of surface excitations at a single surface crossing of an electron, TrMFP (transport mean free path), characteristic to the elastic electron scattering, DIIMFP (differential inverse inelastic mean free path)

and DSEP (differential surface excitation parameter) distributions providing the probability of losing a given energy as a consequence of a bulk or surface excitation. IMFP, SEP, DIIMFP and DSEP can be derived from high energy resolution spectroscopy of electrons backscattered from solid surfaces and examples for the energy dependence of IMFP and SEP in the high electron energy region are mentioned below. As it will also be shown, the TrMFP can be calculated from atomic data available for differential cross section for elastic electron scattering. Here we assume that the DIIMFP and DSEP are dependent on the electron energy in the high energy range only little.

3. Photoemission theories

Among the recently available theoretical methods applicable for describing photoemission induced by high energy (2-15 keV) photons, the method of multipole power series expansion of photon field [1] is used commonly. This model, however, uses a limited number of terms of the expansion, the first term describes the electric dipole operator, the second the electric quadrupole, the third the magnetic dipole, and the fourth term again the electric dipole operator. The irreducible tensor expansion of the photon fields method, developed by Fujikawa et al. [2, 3], at the same time includes all electric dipole operators, as well as other multipole terms. Calculations using these models indicate that in addition to the electric dipole, electric quadrupole and magnetic dipole transitions play important roles in the case of using high-energy X-rays for excitation of photoelectrons. As a consequence of the mutual extinction of effects caused by various errors of different sources, the simpler method based on multipole power series expansion of photon fields [1] still works well in many cases [2].

4. High energy photoemission: nondipole effects influencing the angular distribution of the photoelectrons

The differential photoionization cross section for a linearly polarized photon beam is given by Cooper [4] as

$$\frac{\sigma}{4\pi} \left[1 + \beta P_2(\cos \theta) + (\delta + \gamma \cos^2 \theta) \sin \theta \cos \varphi \right] \quad (1)$$

where σ is the total photoionization cross section, $P_2 = 1/2 (3x^2 - 1)$, θ the angle between the direction of the detected photoelectron and the polarization vector, φ the angle between the direction of photon propagation and the projection of the photoelectron wave vector in the plane perpendicular to the polarization vector, β (dipole), γ and δ (nondipole) are asymmetry parameters. For circularly polarized or unpolarized photons, in eq. (1) β is replaced by $-\beta/2$, θ by $\underline{\theta}$, γ by $\gamma/2$, $\cos^2 \theta$ by $\sin^2 \underline{\theta}$, $\sin \theta \cos \varphi$ by $\cos \underline{\theta}$; where $\underline{\theta}$ is the angle between the directions of the photons and photoelectrons. In eq. (1), δ is usually very small. The asymmetry parameter γ depends on a ratio characterizing the relative contribution of the quadrupole term compared to the dipole one as well as on the corresponding phase shifts of the absorbing atom A [2] (for s levels):

$$\gamma = 18 \frac{\rho_s(2)}{\rho_s(1)} \cos(\delta_1^A - \delta_2^A) \quad (2)$$

where the phase shifts ($l=1,2$) are denoted by δ_l^A and the radial integrals ($l=1,2$) are given as

$$\rho_s(l) = \int R_l(kr) [j_{l-1}(qr) + j_{l+1}(qr)] \frac{dR_s(r)}{dr} r^2 dr$$

where \mathbf{k} and \mathbf{q} are the momentum vectors of the photoelectron and the photon, respectively, R_l is the radial part of the photoelectron wave function with angular momentum l , and j_l is the respective spherical Bessel function. The relative importance of the $E2$ transition compared to the $E1$ transition is indicated by the quantity $\rho_s(2) / \rho_s(1)$. In the case of the Ar 1s photoelectron line, in excellent agreement with the experimental data, the irreducible tensor expansion model predict a change in the value of the γ parameter from about -0.2 to about 0.9 in the photon energy range between 3750 eV and 5500 eV [3]. As for the 2s photoelectrons excited from Ne, Ar and Kr atoms, the relative importance of the quadrupole transition is first decreasing, then – following a minimum (0) value – increasing as a function of photon energy in the range of 100 eV-7000 eV [2]. The angular position of the maximum intensity of the Ne 1s photoelectron angular distribution shifts about 20 deg changing the photon energy from 1 keV to 10 keV and this

shift in the case of the Ne 2*p* photoelectrons is almost 90 deg [2]. The angular distribution of the Ge 2*s* photoelectrons is shown in Fig. 1., as a function of photon energy, the cross section data are taken from Ref. [1]. It can be seen, that the photon energy dependent changes in asymmetry are not even monotonous ones.

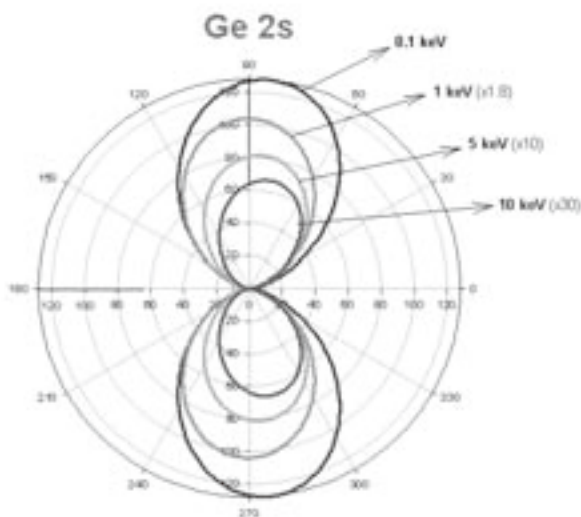


Fig.1. Angular distributions of Ge 2*s* photoelectrons, shown as a function of the exciting photon energy (based on the data from Ref. 1.). The energy values indicated refer to the kinetic energy of the photoelectrons.

Fig. 2. shows the much different angular distributions of the Au 4*f*_{7/2} photoelectrons, as a function of photon energy, the cross section data are again taken from Ref. [1].



Fig. 2. Angular distributions of Au 4*f*_{7/2} photoelectrons, shown as a function of the exciting photon energy (based on the data from Ref. 1.). The energy values indicated refer to the kinetic

energy of the photoelectrons.

The shift in the angular position of the intensity maxima of the photoelectron angular distributions - increasing the photon energy - is quickly increasing, however, it is dependent strongly on the particular atom and subshell as well [1]. Fig. 3. shows the angles corresponding to the maximum intensity photoelectron peak in the angular distribution, as a function of the kinetic energy of the photoelectrons, for different elements and subshells. Large and increasing deviations in angular shifts can be observed with increasing electron energy. In addition to the quadrupole transitions, octupole transitions also can play a non-negligible role. For example, in the case of 1*s* shells of elements Li - Ne, the contribution from octupole transitions is 1-2 % at 5 keV photoelectron kinetic energy and 1.6-3.4 % at 10 keV, using unpolarized photons, while using linearly polarized radiation, the respective values are 5.6-6.0 % ($E_{\text{kin}} = 5 \text{ keV}$) and 8.1-10.6 % ($E_{\text{kin}} = 10 \text{ keV}$) [5].

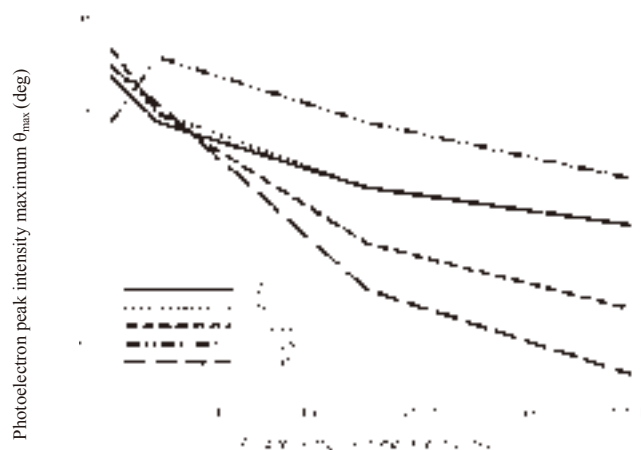


Fig. 3. The angles of the maximum photoelectron peak intensity in the angular distributions, given for different elements and subshells, as a function of the kinetic energy of the photoelectrons.

5. High energy photoemission: effects of atomic recoil

When energetic photoelectrons are emitted especially from low atomic number atoms, the effects of atomic recoil become observable. The recently developed model [6,3] for including such effects uses single site approximation for describing phonon excitations by the recoiled X-ray absorbing atom in a solid and Debye approximation for calculating the energy shift E_r and the peak broadening ΔE_r . According to this model

$$\bar{E}_r = -\frac{Q^2}{2M} \quad (3)$$

where $Q = q - k$ and , denoting the electron binding energy of the respective atomic subshell by E_B and the photon energy by $\hbar\omega$,

$$(\Delta E_r)^2 = \frac{Q^2(k_B T)^2}{2M\omega_D} \int_0^{\theta/T} dx x \frac{e^x - 1}{e^x + 1} + \frac{M\omega_D^3 \delta u^2}{\pi^4} \int_0^{\theta/T} dx \sin^4\left(\frac{\pi T x}{2\theta}\right) \frac{e^x + 1}{x(e^x - 1)} \quad (4)$$

Here θ denotes the Debye temperature, M the atomic mass, δu the nuclear displacement after the core-hole production.

$$\frac{\hbar\omega_D}{k_B T} = \frac{\theta}{T} \quad (5)$$

and the full width at half maximum of the energy distribution broadening the photopeak due to atomic recoil is $FWHM = 2.35 \sqrt{\langle (\Delta E_r)^2 \rangle}$. Using this model, the estimated values for E_r are 0.6 eV (Li 1s), 0.3 eV (C 1s), 0.1 eV (Si 1s) exciting by 5 keV energy photons, while at 10 keV photon energy the corresponding values are 1 eV (Li 1s), 0.5 eV (C 1s) and 0.2 eV (Si 1s), indicating that these energy shifts are comparable to the chemical shifts. The values of the temperature dependent ΔE_r energy broadenings due to atomic recoil vary between 0.1 eV and 0.3 eV for Li 1s photoelectrons using 10 keV energy photons for excitation and temperatures up to 500 K, while in the case of C 1s photoelectrons (from graphite) this broadening varies between 0.1 eV and 0.2 eV in the same range of temperatures, and the same photoline in diamond has a somewhat larger broadening, depending on the temperature only very little [3].

6. Accounting for effects of elastic electron scattering on high energy photoelectron spectra

The differential photoionization cross section of the photoelectrons excited from the nl atomic subshell is given by

$$\frac{d\sigma_{nl}}{d\Omega} = \frac{F\sigma_{nl}}{4\pi} \quad (6)$$

where σ_{nl} is the total subshell photoionization cross section and F is an angular dependent factor described in eq. (1) for linearly polarized photons. In the case of solids, however, the elastic scattering of the photoelectrons within the material distorts their angular distribution, so, for high energy photoelectrons emitted from solids a similar factor F_s is recommended to be used [7]:

$$F_s = a \left[D_1 - \frac{\beta}{4} (3 \cos^2 \theta - 1) + \left(\frac{\gamma}{2} \sin^2 \theta + \delta \right) \cos \theta \right] \quad (7)$$

where $a = 1 - \omega$, and here ω denotes the single scattering albedo

$$\omega = \frac{\lambda}{\lambda_{tr} + \lambda}$$

with λ as the inelastic mean free path of electrons in the solid (IMFP), λ_{tr} the transport mean free path of the electrons

$\lambda_{tr} = (M\sigma_{tr})^{-1}$; $\sigma_{tr} = \int_{4\pi} (1 - \cos\theta)(d\sigma/d\Omega)d\Omega$ where M denotes atomic density and $d\sigma/d\Omega$ the differential cross section for elastic electron scattering within the material. Furthermore, in eq. (7)

$$D_1 = H(\mu, \omega)(1 - \omega)^{0.5}$$

where $\mu = \cos \alpha$ (α : angle of photoelectron emission) and

$$H(\mu, \omega) = \frac{1 + 1.908\mu}{1 + 1.908\mu(1 - \omega)^{0.5}}$$

(an approximation of the Chandrasekhar function). The strength of the effects of the elastic scattering on the high energy photoelectron spectra in the case of an overlayer of a particular material can be estimated from the ratio of the effective attenuation length (EAL) of the electrons within the layer to the IMFP as a function of the electron energy. EAL represents the characteristic length in the formula describing the exponential attenuation of the intensity of the photoelectrons emitted from the overlayer, accounting for effects of elastic electron scattering as well. Although EAL depends on the angle of emission and on the thickness of the overlayer, it is nearly constant in a broad range of emission angles and layer thicknesses. The general formula proposed by Seah and Gilmore [8a]

gives the mentioned ratio as

$$EAL_{SG}/\lambda = 0.979[1-\omega(0.955-0.0777)\ln Z] \quad (8)$$

where Z denotes the atomic number and the formula is calculated for a photoelectron emission angle of 45° and recommended for of emission angles between 0° and 58° . Calculated using the formula (8) for homogeneous overlayers in the case of different elements, the EAL_{SG}/λ ratio (depending on the atomic number) increases with electron kinetic energy and shows a saturation at about 6 keV, indicating a strongly decreased role of the elastic electron scattering for higher energy photoelectrons (Fig. 4.). The ratios calculated using the formula (8) above are in a close agreement with the data derived from the NIST SRD 82 database [8b].

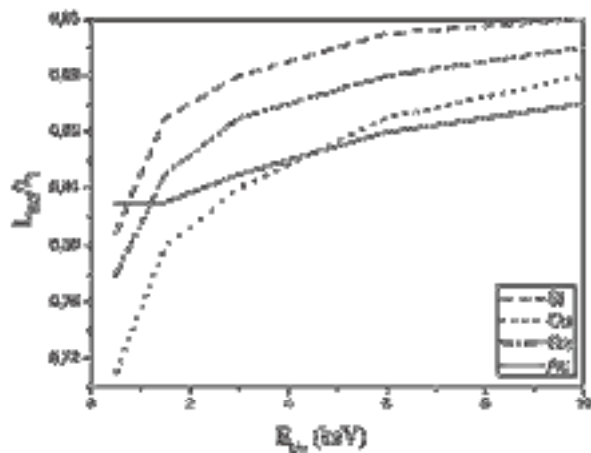


Fig. 4. The ratio of the effective attenuation length (EAL) to the IMFP (λ) given by the formula of Seah and Gilmore [8a] as a function of the electron energy, for different elements.

7. Energy dependence of inelastic electron scattering

Accompanying photoionization, different excitations can take place resulting in energy losses of the photoelectrons. Upon creation of hole(s) via shake up/off processes electrons in occupied bound states are excited to unoccupied electronic states and collective (plasmon) excitations can occur (intrinsic excitations). During the electron transport within the solids, electrons can lose energy due to plasmon excitations in the bulk or at the surface (extrinsic excitations). Multiple excitations are probable and interferences between surface and bulk, as well as between intrinsic and extrinsic excitations can often appear. The probability of such excitations and the distribution of the probabilities in the case of multiple

excitations can be characterized with the corresponding transport parameters. In the case of bulk excitations an important characteristic parameter is the IMFP, its dependence on the electron energy E can be approximated with the simple expression [9]:

$$\lambda = k E^p, \text{ where } k \text{ and } p \text{ are material dependent constants.}$$

In the case of polycrystalline Ge, e.g. the IMFP derived from Elastic Peak Spectroscopy using the model based on the Monte Carlo simulation of electron scattering in solids, shows a significant, a factor of 3 increase changing the electron energy from 2 keV to 10 keV, reaching a value of ca. 11 nm [10]. The average number of surface excitations in a single surface crossing of an electron having a given energy and direction, the Surface Excitation Parameter (SEP) is characterizing the probability of surface excitations, which follows a Poisson statistics for multiple surface excitations. The SEP depends on the inverse square root of the electron energy [11], e.g. in the case of Reflection Electron Energy Loss Spectroscopy (REELS) changing the primary electron energy from 100 eV to 5 keV, at an angle of incidence (primary electron beam) of 0° and angle of emission of 60° related to the surface normal, the SEP decreases by a factor of about 5 in the case of Au and Cu [12].

For probabilities of extrinsic and intrinsic, surface and bulk excitations, information can be obtained from the analysis of hard X-rays induced photoelectron and Auger spectra as well, using different models for spectral interpretation. These models, e. g. the simple empirical Modified Hüfner (MH) model [13, 14] and the more sophisticated Partial Intensity Analysis (PIA) model – based on the independence of different type (bulk, surface and intrinsic) excitations – developed by Werner [15-17] and the semiclassical Dielectric Response (DR) model developed by Yubero and Tougaard [18-20] can provide the corresponding electron transport parameters. Applying these models to the interpretation of the Ge $2s$ photoelectron spectra excited by 8 keV energy photons from a polycrystalline Ge layer, it can be seen that the MH and the PIA models provide very similar intrinsic spectra, while the DR model predicts a much larger probability for intrinsic excitations [13]. The MH and PIA models are based on similar assumptions regarding the independence of different type excitations, with the major difference that the parameters related to the probabilities of the various type excitations are derived by fitting in

the case of the MH model while in the case of the PIA model they can be obtained from Monte Carlo simulation of electron scattering (bulk excitations) or from independent experiments (surface excitations). Looking at the dependence of the first partial intensities on the kinetic energy of the Ge 2s photoelectrons, our results [21] show that while the probability of the surface excitation is decreasing with electron energy, the probability of the intrinsic excitations is increasing. The findings above suggest the partial invalidity of the assumption on the independence of the different type excitations. Based on previous results [22] recent works [23] try to explain these tendencies assuming a destructive interference between the extrinsic and intrinsic excitations, with a probability inversely proportional to the electron velocity and decreasing with increasing order of multiple plasmon excitation.

8. Quantitative information on electronic structure of 3d metals from (non-resonant and resonant) Auger spectra excited by hard X-rays

It is possible to obtain quantitative information on the density of the unoccupied electronic states in the case of resonantly photoexcited core Auger spectra of 3d transition metals [24-26]. For Cu and Ni, these studies confirmed the existence of both initial-state and final state shake up excitations to unoccupied bound states, through the analysis of the intensity evolution of the satellite peaks in the resonant KLL Auger spectra and showing a good agreement between the satellite evolution curves obtained experimentally and predicted by theoretical models for initial state shake up processes [24]. Analyzing the changes in the Resonant Raman KLL Auger spectra of Cu and Ni metals as a function of exciting photon energy, and comparing the experimental spectra (obtained using thick and nanolayer samples) to model spectra, direct information can be obtained on the density of the unoccupied 4p states [25, 26]. The model for interpreting these Auger Resonant Raman lineshapes – and providing a good agreement [25,30] with the experimental spectra – is based on the resonant X-ray scattering theory [27], the DV-X α cluster molecular orbital model [28] for deriving the partial density of the unoccupied 4p states and on the dielectric response model [29] describing the energy losses due to surface, bulk, extrinsic and intrinsic excitations [30]. An example for obtaining

quantitative electronic structure information from non resonant deep core Auger spectra, is the case of the Ni KLM Auger spectra photoexcited from metallic Ni [31]. Using the Partial Intensity Analysis method for describing the energy loss parts of the spectra and comparing the determined Auger transition energies and relative Auger peak intensities obtained experimentally to those derived from various atomic models, our results clearly show the validity of the intermediate coupling model for the Ni KLM transitions [31].

9. Summary

Non-dipole effects in hard (5-10 keV) X-rays induced photoelectron spectroscopy result in significant changes in the angular distribution of photoelectrons. Energy shifts of photoelectron peaks of low atomic number components, due to atomic recoil, can be comparable to chemical shifts, while the related (Doppler-) energy broadenings can influence the accuracy of the quantitative analysis. Elastic electron scattering and surface excitations have a decreasing role at increasing, high electron energies. Interferences between bulk intrinsic and extrinsic excitations are expected to decrease with increasing photoelectron kinetic energy, improving the conditions for applications of models assuming the independence of these excitations. Examples are provided for obtaining quantitative electronic structure information from hard X-rays excited photoelectron (Ge 2s), resonant (Cu, Ni KLL) and non resonant (Ni KLM) spectra of solid samples.

10. Acknowledgements

The financial support of the Hungarian grant OTKA K 67873 and of the DESY/HASYLAB and the European Community under Contract RII3-CT-2004-506008 (IA-SFS), as well as the support of the Hungarian Academy of Sciences and the Japanese Society for Promotion of Science is gratefully acknowledged.

11. References

- [1] M.B. Trzhaskovskaya, V.I. Nefedov, V.G. Yarzhevsky, Atomic Data and Nuclear Data Tables 77, 97 (2001); 82, 257 (2002); 92, 345 (2006).
- [2] T. Fujikawa, R. Suzuki, H. Arai, H. Shinotsuka, L. Kövér, J. Electron Spectrosc. Relat. Phenom. 159, 14 (2007).

- [3] R. Suzuki, H. Arai, H. Shinotsuka, T. Fujikawa, e-J. Surf. Sci. Nanotech. 3, 373 (2005).
- [4] J. W. Cooper, Phys. Rev. A47, 1841 (1993).
- [5] M.B. Trzhaskovskaya, V.I. Nefedov, V.G. Yarzhemsky, R. Szargan, J. Electron Spectrosc. Relat. Phenom. 133, 65 (2003).
- [6] T. Fujikawa, R. Suzuki, L. Kövér, J. Electron Spectrosc. Rel. Phenom. 151, 170 (2006).
- [7] V.I. Nefedov, V.G. Yarzhemsky, R. Hesse, P. Streubel, R. Szargan, J. Electron Spectrosc. Relat. Phenom. 125, 153 (2002).
- [8a] M.P. Seah, I. Gilmore, Surf. Interface Anal. 31, 835 (2001).
- [8b] C. J. Powell, A. Jablonski, W. S. M. Werner, W. Smekal, Appl. Surf. Sci. 239, 470 (2005).
- [9] C. J. Powell, A. Jablonski, J. Phys. Chem. Ref. Data 28, 19 (1999).
- [10] Z. Berényi, B. Aszalós-Kiss, J. Tóth, D. Varga, L. Kövér, K. Tökési, I. Cserny, S. Tanuma, Surf. Sci. 566-568, 1174 (2004).
- [11] W. S. M. Werner, W. Smekal, C. Tomastik, H. Störi, Surf. Sci. 486, L461 (2001).
- [12] K. Salma, Z. J. Ding, H. M. Li, Z. M. Zhang, Surf. Sci. 600, 1526 (2006).
- [13] L. Kövér, M. Novák, S. Egri, I. Cserny, Z. Berényi, J. Tóth, D. Varga, W. Drube, F. Yubero, S. Tougaard and W.S.M. Werner, Surf. Interface Anal. 38, 569 (2006).
- [14] M. Novák, L. Kövér, S. Egri, I. Cserny, J. Tóth, D. Varga, W. Drube, J. Electron Spectrosc. Relat. Phenom. 163, 7 (2008).
- [15] W.S.M. Werner, Surf. Interface Anal. 31, 141 (2001).
- [16] W.S.M. Werner, L. Kövér, J. Tóth, D. Varga, J. Electron Spectrosc. Rel. Phenom. 22, 103 (2002).
- [17] W.S.M. Werner, L. Kövér, S. Egri, J. Tóth, D. Varga, Surf. Sci. 585, 85 (2005).
- [18] F. Yubero, S. Tougaard, Phys. Rev. B46, 2486 (1992).
- [19] A. Cohen-Simonsen, F. Yubero, S. Tougaard, Phys. Rev. B56, 1612 (1997).
- [20] F. Yubero, S. Tougaard, Phys. Rev. B71, 045414 (2005).
- [21] M. Novák, S. Egri, L. Kövér, I. Cserny, W. Drube, W. S. M. Werner, Surf. Sci., 601, 2344 (2007).
- [22] J. J. Chang, D. C. Langreth, Phys. Rev. B8, 4633 (1973).
- [23] C. Biswas, A. K. Shuklin, S. Banik, V. K. Ahire, S. R. Barman, Phys. Rev. B67, 165416 (2003).
- [24] L. Kövér, Z. Berényi, I. Cserny, L. Lugosi, W. Drube, T. Mukoyama, V. R. R. Medicherla, Phys. Rev. B73, 195101 (2006).
- [25] L. Kövér, W. Drube, Z. Berényi, I. Cserny, V. R. R. Medicherla, T. Ishii, H. Ikeno, H. Adachi, Surf. Sci. 601, 1085 (2007).
- [26] L. Kövér, I. Cserny, W. Drube, M. Novák, S. Egri, HASYLAB Annual Report 2006, 1027 (2007).
- [27] W. Drube, T. M. Grehk, R. Treusch, G. Materlik, Phys. Rev. Lett. 74, 42 (1995).
- [28] H. Adachi, M. Tsukada, C. Satoko, J. Phys. Soc. Jpn. 45, 875 (1978).
- [29] F. Yubero, S. Tougaard, Phys. Rev. B46, 2486 (1992); A. Cohen-Simonsen, F. Yubero, S. Tougaard, Phys. Rev. B56, 1612 (1997); F. Yubero, S. Tougaard, Phys. Rev. B71, 045414 (2005).
- [30] L. Kövér, I. Cserny, W. Drube, F. Yubero, S. Tougaard, to be published.
- [31] S. Egri, L. Kövér, W. Drube, I. Cserny, M. Novák, J. Electron Spectrosc. Relat. Phenom. 162, 115 (2008).